Journal of
Low Power Electronics
Vol. 15, 51–63, 2019

Complete Study for Diagonal Triboelectric Nanogenerators Based Energy Harvester with Computer Aided Design Tool

Endy Onsy[1,†], Reem Abd El-Sttar[1,†], George S. Maximous[2], Ahmed Zaky[1], and Hassan Mostafa[1,3,*]

[1] *University of Science and Technology, Nanotechnology and Nanoelectronics Program, Zewail City of Science and Technology, October Gardens, 6th of October, Giza 12578, Egypt*
[2] *Department of Electrical Engineering, British University in Egypt, Cairo 11837, Egypt*
[3] *Electronics and Communication Department, Faculty of Engineering, Cairo University, Giza 12613, Egypt*

(Received: 18 December 2018; Accepted: 10 February 2019)

In the past few years, electrical energy harvesting from the ambient environment has attracted much of the research interests due to the increasing need for energy resources that suit the rapid development of power electronic devices. Recently, a novel mechanical energy harvesting and transduction technology has been introduced called the triboelectric nanogenerators (TENGs), with many advantages over the other harvesters. In this work, a new diagonal motion mode for TENGs is studied intensively in the attached electrode regime and simulated using COMSOL MULTIPHYSICS. The diagonal motion mode offers a new way of motion represented in the angle theta (θ)—between the left endpoint of the bottom dielectric and the left endpoint of the top dielectric—that ranges from 0 to 90 degrees, and allows for further energy optimization. A complete analytical model of the proposed TENG structure has been derived step by step, and its results were compared to COMSOL simulation results to validate its accuracy. The maximum error between the results is equal to 5.3%, 4.3% and 0.88% for the open circuit voltage (V_{OC}), short circuit charge (Q_{SC}) and Capacitance (C) respectively. Based on the developed model, a performance optimization study has been performed on the dielectric material used in the device. The study revealed that, the tribo-pair of Nylon and Kapton corresponds to the best performance of the harvester amongst the other pairs used in the literature with a maximum energy of 0.40118 nJ. In addition to this, the accuracy of the analytical model was a motivation for constructing a Verilog-A model, by which the device was studied under different loading conditions such as simple resistive and capacitive loads. Finally, a MATLAB based CAD tool has been developed to allow rapid prototyping and testing of different device parameters on the device performance.

Keywords: Diagonal TENGs, Triboelctric, Nanogenerators, COMSOL, Energy Harvesting, Device Modeling, Verilog-A, Performance, CAD Tool.

1. INTRODUCTION

During the last decades, the electronics industry has been revolutionized and greatly developed leading to the drastic increase of the number of portable electronic devices. This rapid growth in the energy demand has triggered a great problem as the widely used batteries have limited lifetimes and pose great environmental hazards. As the portable and wearable electronics consume low power, the notion of scavenging and using energy directly from the local environment has been regarded as a promising alternative to compensate for the lack of traditional fuel sources and to enable the design of self-sufficient systems.[1,2]

Mechanical energy has gained the attention as the most suitable form of energy to be harvested due to its abundance and minimal contamination to the environment. Various technologies have been developed to harvest the mechanical energy such as piezoelectric, electromagnetic and electret harvesters, each with its advantages and its drawbacks.[3,4] The piezoelectric harvesters, for example, are based upon the property of piezoelectricity that some materials possess, which is the ability of the material to generate an electric voltage across it when subjected to a mechanical stress. The most common configuration for piezoelectric energy harvesting is based upon cantilevers

*Author to whom correspondence should be addressed.
Email: hmostafa@zewailcity.edu.eg
†These two authors contributed equally to this work.

that are subjected to cyclic forces and thus generate cyclic voltages.[5] Additionally, a proof mass can be added at the tip of the cantilever to improve the performance of the harvester through increasing the stress magnitude. The main disadvantage of the cantilever-based design is its limited frequency range for operation because of its dependence on the natural resonance of the structure. Other than the cantilever designs, circular diaphragms, cylindrical shells and many other configurations were developed as piezoelectric energy harvesters that operate in a similar manner to cantilevers and use a proof mass to provide a pre-stress.[6] Piezoelectric energy harvesters have the drawbacks of generating low output power and using a limited number of materials that are relatively expensive and sensitive to the temperature and require complex fabrication techniques.[7, 8] Electromagnetic harvesters utilize Faraday's law that states that the emf (electromotive force) is directly proportional to the flux enclosed in a closed loop; however, the fabrication of coils and magnets becomes very challenging as the dimensions of the devices decrease.[7] On the other hand, one of the least used energy harvesters due to their low output power is the electrostatic one that uses variable parallel plate capacitors, as mechanical motion leads to variation in the relative distance between the two plates and thus the capacitance value.[7] One of its most common types depends on electrets (dielectric materials that are permanently polarized) to create potential difference between the two plates.[9]

However, in 2012 a new technology termed the triboelectric nanogenerator (TENG) has been developed that overcomes most of the drawbacks of the other types of harvesters and offers many advantages such as its light weight, low cost, high output power, high efficiency and easy fabrication.[10] In addition, it can harvest various forms of mechanical energy such as: human motion, water flow, wind and tire rotation.[11] TENGs combine two of the most common physical phenomena which are the triboelectrification and electrostatic induction.[12] Triboelectrication is the phenomenon of generation of electric charges when two different materials come in contact with each other,[13] while electrostatic induction is the redistribution of charges inside the materials in response to the nearby charges. The triboelectric effect generates static charges on the inner sides of the tribo-pair, then the static charges induce mobile ones on the opposite sides of the electrodes that flow when a potential difference arises between the metals as a result of separating the tribo-pair, thus converting the mechanical energy to electrical one.[14] Triboelectric nanogenerators have three types which are attached electrode, single electrode and freestanding layer with each type having certain structure and triggering order.[15] The attached electrode type is characterized by its electrodes being on the outer side of the structure while the rest of the layers are sandwiched between them with the conductor and the dielectric of each half being attached to each other as shown in Figure 1(a). While the single electrode type has one of its dielectrics as the outer surface and the layers are detached as shown in Figure 1(b) and the freestanding layer type is similar to the attached electrode regarding the placement of the electrodes but with each layer separated as shown in Figure 1(c). For every type, there are two basic modes: Contact mode and sliding mode. The mode represents the motion scenario of TENG, in which it moves in a vertical direction for the contact mode and in horizontal lateral direction for the sliding mode. A new mode of operation called the diagonal mode which is considered a hybrid mode between both contact and sliding modes has been proposed before.[16] The diagonal mode offers a new degree of freedom and can be used in various applications; however, no analytical model has been developed for it, only the curve-fitting equations have been used.

In this study, the proposed attached electrode diagonal mode is presented in Section 2, and its detailed analytical model is proposed and derived step by step in 2.1. The COMSOL MULTIPHYSICS model is shown in 2.2. Moreover, the effect of dielectric materials on its performance has been elucidated and tested on unidirectional charging for a capacitor, which serves as an important step in diagonal TENGs fabrication, is presented in 2.3.1 and 2.3.2. Furthermore, a Verilog-A model is introduced in 2.4, which is developed to study the device performance with various loads such as resistors and capacitors. In Section 3, a CAD tool is proposed, which is designed with different features to substitute for the long time FEM simulations of the diagonal TENG. Results are discussed in Section 4, then finally the conclusion and the future work are presented in Section 5.

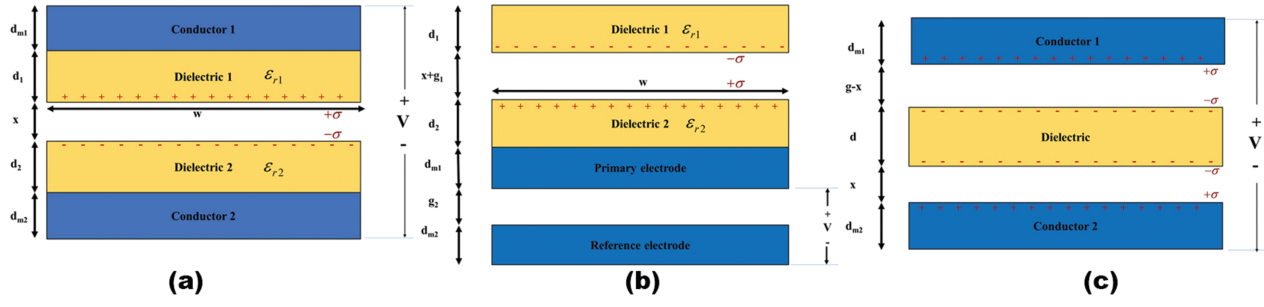

Fig. 1. (a) Attached electrode mode, (b) single electrode mode and (c) freestanding electrode mode.

2. PROPOSED DIAGONAL MODEL

The diagonal mode of the attached electrode TENG has been proposed before.[16, 17] The basic structure is similar to the attached electrode fundamental modes (contact and sliding modes), so it can be conductor-dielectric structure or dielectric–dielectric structure depending on the materials of the triboelectric pair. However, the diagonal mode differs mainly in its movement scenario. It offers a new degree of freedom as it moves with an angle theta ranging from 0 to 90 degrees, instead of moving only in the horizontal or the vertical direction. The diagonal mode structure is shown in Figure 2, in which theta is measured from the left endpoint of the bottom dielectric to the left endpoint of the top dielectric.

Throughout the following discussion, the dielectric–dielectric structure shall be addressed and explained thoroughly as the same concepts are applied to the conductor-dielectric structure with minor differences. It consists of four layers: two dielectrics and two metals. The two dielectrics are the tribo-pair between which the charge transfer takes place. As a result of contact electrification, static charges of equal density and opposite polarity ($+\sigma$ and $-\sigma$) arise across the surfaces of the two dielectrics. Thereafter, as the tribo-pair gets separated by a mechanical force, a potential difference (V_{oc}) arises between the two metals such that when they are electrically connected to each other, charges of magnitude Q are transferred between them to balance this potential difference. Meanwhile if the separation distance is decreased, this potential difference shall decrease. So, the voltage between the two electrodes is controlled by two parts: the first is from the static polarized charges on the dielectrics, setting a potential difference of $V_{oc}(\theta)$ across the electrodes. The other one is from the inherent capacitance of the structure with Q charges transferred thus contributing a voltage equals to $-Q/C(\theta)$. By using the superposition principle, the voltage difference across the two electrodes is given by:

$$V = \frac{-Q}{C(\theta)} + V_{OC}(\theta) \tag{1}$$

Accordingly, both $V_{oc}(\theta)$ and $C(\theta)$ should be acquired to fully describe the model and achieve a closed form $(V - Q - \theta)$ relation. Moreover, it has been shown before in Ref. [16] that air insulation drastically improves the performance of the diagonal mode compared to the other fundamental modes of motion, so the structure has been air insulated in this study.

2.1. Analytical Model

The attached electrode diagonal mode with air insulation is equivalent to four capacitors connected in parallel as shown in Figure 3: one between the upper and bottom electrodes (C_1), one between the upper electrode and the right wall (C_2), one between the upper electrode and the left wall (C_3) and one between the upper electrode and the upper wall (C_4). Therefore, the total charge on the four capacitors is the summation of the charges on each capacitor.

$$Q_{SC} = Q_{SC_1} + Q_{SC_2} + Q_{SC_3} + Q_{SC_4} \tag{2}$$

And according to the TENG governing equation shown in Eq. (1):

$$Q_{SC} = V_{OC} \times C \tag{3}$$

So,

$$Q_{SC} = V_{OC_1} C_1 + V_{OC_2} C_2 + V_{OC_3} C_3 + V_{OC_4} C_4 \tag{4}$$

V_{oc} of each capacitor can be derived by thoroughly understanding the charge distribution. At the non-overlapped region of the structure, the dielectric induces an equal and opposite charge on the conductor. And the charge at the overlapped region is determined by the fact that under OC condition, the total charges on each conductor should be zero.

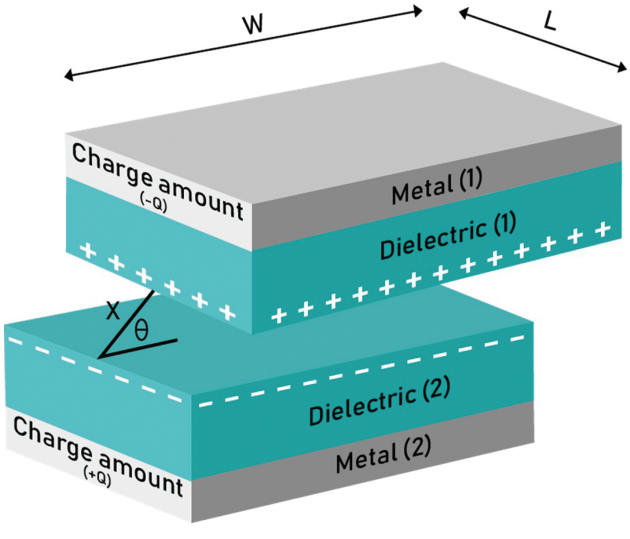

Fig. 2. Proposed diagonal mode configuration in 3D.

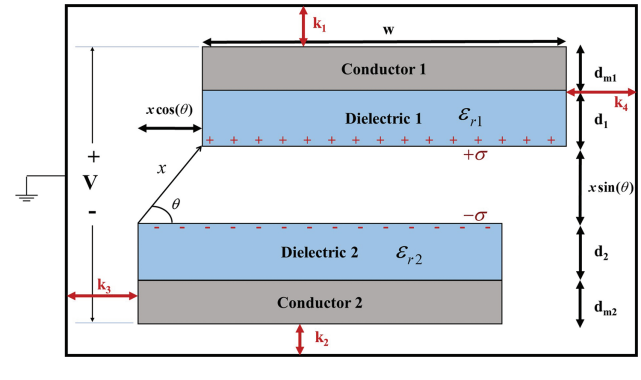

Fig. 3. The 2D model of the air-insulated dielectric–dielectric diagonal TENG.

Assume charge densities of A and B on the overlapping regions of the top and bottom electrodes respectively as in Refs. [18, 19], then to satisfy OC condition:

$$\sum Q_{\text{top}} = -\sigma x\cos(\theta)l + A(w - x\cos(\theta))l = 0 \quad (5)$$

$$\sum Q_{\text{bottom}} = \sigma x\cos(\theta)l + B(w - x\cos(\theta))l = 0 \quad (6)$$

In which, w and l are the device width and length respectively, σ is the surface charge density and x is the diagonal distance. Therefore, A and B equal:

$$A = \frac{\sigma x\cos(\theta)}{(w - x\cos(\theta))}, \quad B = \frac{-\sigma x\cos(\theta)}{(w - x\cos(\theta))} \quad (7)$$

For the first capacitor between the first and second conductor, the electric field is in the z-direction and is found by applying Gauss's law in each of the five regions of the top conductor, first dielectric, the air gap, the second dielectric and the bottom conductor:[16, 19, 20]

$$\oint E \cdot dA = \frac{Q_{\text{enclosed}}}{\varepsilon_0} \quad (8)$$

Where, E is the electric field, dA is the infinitesimal element of the surface area, Q_{enclosed} is the charge enclosed within the chosen surface and ϵ_0 is the Vacuum permittivity.

First, E_1 which is the electric field inside the top conductor is derived as follows,

$$-E_1(w - x\cos(\theta))l = \frac{A(w - x\cos(\theta))l}{\varepsilon_0} \quad (9)$$

Hence E_1 equals to:

$$E_1 = \frac{-A}{\varepsilon_0} = \frac{-\sigma x\cos(\theta)}{\varepsilon_0(w - x\cos(\theta))} \quad (10)$$

Then, E_2 which is the electric field inside the first dielectric is derived as follows,

$$-E_2(w - x\cos(\theta))l = \frac{A(w - x\cos(\theta))l}{\varepsilon_0\varepsilon_{r1}} \quad (11)$$

In which ϵ_{r1} is the permitivity of the first dielectric. Hence E_2 equals to:

$$E_2 = \frac{-A}{\varepsilon_0\varepsilon_{r1}} = \frac{\sigma x\cos(\theta)}{\varepsilon_0\varepsilon_{r1}(w - x\cos(\theta))} \quad (12)$$

Then, E_3 which is the electric field inside the air gap is derived as follows,

$$-E_3(w - x\cos(\theta))l = \frac{A(w - x\cos(\theta))l}{\varepsilon_0} + \frac{\sigma(w - x\cos(\theta))l}{\varepsilon_0} \quad (13)$$

Hence E_3 equals to:

$$E_3 = -\frac{A}{\varepsilon_0} - \frac{\sigma}{\varepsilon_0} = -\frac{\sigma x\cos(\theta)}{\varepsilon_0(w - x\cos(\theta))} - \frac{\sigma}{\varepsilon_0} \quad (14)$$

Then, E_4 which is the electric field inside the second dielectric is derived as follows,

$$E_4(w - x\cos(\theta))l = \frac{B(w - x\cos(\theta))l}{\varepsilon_0\varepsilon_{r2}} \quad (15)$$

In which ϵ_{r2} is the permitivity of the second dielectric. Hence E_4 equals to:

$$E_4 = \frac{B}{\varepsilon_0\varepsilon_{r2}} = \frac{-\sigma x\cos(\theta)}{\varepsilon_0\varepsilon_{r2}(w - x\cos(\theta))} \quad (16)$$

Then, E_5 which is the electric field inside the bottom electrode is derived as follows,

$$E_5(w - x\cos(\theta))l = \frac{B(w - x\cos(\theta))l}{\varepsilon_0} \quad (17)$$

Hence E_5 equals to:

$$E_5 = \frac{B}{\varepsilon_0} = \frac{-\sigma x\cos(\theta)}{\varepsilon_0(w - x\cos(\theta))} \quad (18)$$

Regarding V_{OC}, it is determined using the line integral formula found in Ref. [21] as follows:

$$V_{\text{OC}} = -\int_0^{d_{m1}+d_1+x\sin(\theta)+d_2+d_{m2}} E \cdot dz \quad (19)$$

$$\begin{aligned} V_{\text{OC}_1} = &-\int_0^{d_{m1}} E_1 \cdot dz - \int_{d_{m1}}^{d_{m1}+d_1} E_2 \cdot dz \\ &- \int_{d_{m1}+d_1}^{d_{m1}+d_1+x\sin(\theta)} E_3 \cdot dz \\ &- \int_{d_{m1}+d_1+x\sin(\theta)}^{d_{m1}+d_1+x\sin(\theta)+d_2} E_4 \cdot dz \\ &- \int_{d_{m1}+d_1+x\sin(\theta)+d_2}^{d_{m1}+d_1+x\sin(\theta)+d_2+d_{m2}} E_5 \cdot dz \end{aligned} \quad (20)$$

Where d_{m1} and d_{m2} are the thicknesses of the first and second metal electrodes respectively. And d_1 and d_2 are the thicknesses of the first and second dielectrics respectively. By substituting with the derived formulas for the electric field with A and B values as found in Eq. (7), V_{oc_1} yields to:

$$\begin{aligned} V_{\text{OC}_1} = &\frac{\sigma x\cos(\theta)}{\varepsilon_0(w - x\cos(\theta))}(x\sin(\theta) + d_0 + d_{m1} + d_{m2}) \\ &+ \frac{\sigma(x\sin(\theta))}{\varepsilon_0} \end{aligned} \quad (21)$$

With d_0 defined as the dielectric equivalent thickness given by $d_0 = d_1/\varepsilon_{r1} + d_2/\varepsilon_{r2}$.

Since, the overlapping part of the structure is the most dominant part for the capacitance. Hence, the capacitance is given by:

$$C_1 = \frac{\varepsilon_0(w - x\cos(\theta))l}{(x\sin(\theta) + d_0 + d_{m1} + d_{m2})} \quad (22)$$

For the second capacitor between the top electrode and the right wall, the electric field is in the horizontal direction (x'-direction) and is found by applying Gauss's law:

$$E_6 d_{m1} l = \frac{-\sigma d_{m1} l}{\varepsilon_0} \rightarrow E_6 = \frac{-\sigma}{\varepsilon_0} \tag{23}$$

$$V_{OC_2} = -\int_{k_3 + x\cos(\theta) + w}^{k_3 + x\cos(\theta) + w + k_4} E_6 dx' = \frac{-\sigma}{\varepsilon_0} k_4 \tag{24}$$

With k_3 and k_4 defined as the air insulation distances between the bottom electrode and the left wall, and between the upper electrode and the right wall respectively. And the capacitance using the parallel plate capacitor formula is:

$$C_2 = \frac{\varepsilon_0 d_{m1} l}{k_4} \tag{25}$$

For the third capacitor between the top electrode and the left wall, the electric field (in the x-direction) is found by applying Gauss's law:

$$-E_7 d_{m1} l = \frac{A d_{m1} l}{\varepsilon_0} \rightarrow E_7 = \frac{-A}{\varepsilon_0} \tag{26}$$

$$\begin{aligned} V_{OC_3} &= -\int_0^{k_3 + x\cos(\theta)} E_7 dx' \\ &= \frac{\sigma x \cos(\theta)}{\varepsilon_0 (w - x\cos(\theta))} (k_3 + x\cos(\theta)) \end{aligned} \tag{27}$$

And the capacitance is given by:

$$C_3 = \frac{\varepsilon_0 d_{m1} l}{(k_3 + x\cos(\theta))} \tag{28}$$

For the fourth capacitor between the top electrode and upper wall, by applying Gauss's law under OC condition it is found that:

$$E_8 w l = \frac{Q_{\text{enclosed}}}{\varepsilon_0} = 0 \rightarrow E_8 = 0 \tag{29}$$

Hence, $V_{OC_4} = 0$ and the capacitance is found to be:

$$C_4 = \frac{\varepsilon_0 w l}{k_1} \tag{30}$$

here, k_1 is the air insulation distance between the upper electrode and the upper wall. Therefore, by using Eqs. (4), (21), (22), (24), (25), (27–30), Q_{SC} is found to be:

$$\begin{aligned} Q_{SC} = \sigma l x \cos(\theta) &+ \frac{(\sigma l x \sin(\theta))(w - x\cos(\theta))}{(x\sin(\theta) + d_0 + d_{m1} + d_{m2})} \\ &- \sigma d_{m1} l + \frac{\sigma d_{m1} l x \cos(\theta)}{(w - x\cos(\theta))} \end{aligned} \tag{31}$$

And the total capacitance of the structure is the equivalent of the four parallel capacitors as mentioned earlier:

$$C_{\text{total}} = C_1 + C_2 + C_3 + C_4 \tag{32}$$

$$\begin{aligned} C_{\text{total}} = &\frac{\varepsilon_0 (w - x\cos(\theta)) l}{(x\sin(\theta) + d_0 + d_{m1} + d_{m2})} + \frac{\varepsilon_0 d_{m1} l}{k_4} \\ &+ \frac{\varepsilon_0 d_{m1} l}{(k_3 + x\cos(\theta))} + \frac{\varepsilon_0 w l}{k_1} \end{aligned} \tag{33}$$

And finally V_{OC} can be found as: $V_{OC} = Q_{SC}/C_{\text{total}}$. By substituting with Q_{SC} shown in Eq. (31) and C_{total} shown in Eq. (33), the closed form $(V - Q - \theta)$ relation can be determined as follows:

$$\begin{aligned} V = 1 \Bigg/ &\left(\frac{\varepsilon_0 (w - x\cos(\theta)) l}{(x\sin(\theta) + d_0 + d_{m1} + d_{m2})} + \frac{\varepsilon_0 d_{m1} l}{k_4} \right. \\ &\left. + \frac{\varepsilon_0 d_{m1} l}{(k_3 + x\cos(\theta))} + \frac{\varepsilon_0 w l}{k_1} \right) \\ &\times \left(-Q + \sigma l x \cos(\theta) \right. \\ &+ \frac{\sigma l (x\sin(\theta))(w - x\cos(\theta))}{(x\sin(\theta) + d_0 + d_{m1} + d_{m2})} - \sigma d_{m1} l \\ &\left. + \frac{\sigma d_{m1} l x \cos(\theta)}{(w - x\cos(\theta))} \right) \end{aligned} \tag{34}$$

2.2. COMSOL Model

The finite element method (FEM) software, COMSOL Multiphysics 5.3, was used throughout this study to calculate the open circuit voltage and short circuit transferred charge. Since there is no physics available for the triboelectrification in COMSOL, electrostatics physics and stationary study are used instead, in which static charges of $+\sigma$ and $-\sigma$ were added on the surfaces of the two dielectrics. The two dielectrics used are Nylon and PTFE (Polytetrafluoroethylene), respectively. Table I shows the parameters used in this simulation, however they can be changed according to the application of the TENG.

Both the short-circuit (SC) condition and the open-circuit (OC) condition of the structure were studied intensively. The OC boundary condition requires a zero-total surface charge density on each metal electrode which is satisfied in the model by setting the terminal type as charge and its value $Q_0 = 0$. Regarding the SC boundary condition, a zero-electric potential difference between the two

Table I. Parameter set used throughout COMSOL simulation.

Parameter	Value
Device width and length w, l	1 mm
Diagonal distance x	100 μm
Thickness of the dielectrics d_1, d_2	25 μm
Thickness of the metal electrodes d_m	1 μm
Relative dielectric constants ε_{r1}, ε_{r2}	4, 2
Air insulation distances $k_{1,2,3,4}$	1 μm
Surface charge density σ	100 μC/cm^2
Average angular velocity ω	1 ms^{-1}
Maximum diagonal angle $\theta_{\max}$	90°

metal electrodes is required. This was implemented in the model by choosing the terminal type as voltage and its value $V_0 = 0$. Also, air insulation is applied to surround the structure in this simulation, which is attainable in the real life too.

2.3. Diagonal TENG Performance and Optimization

For any TENG structure, the output optimization can be achieved by specifically choosing the used materials. This section aims at providing insights about choosing the suitable materials which is a rigorous task and is extremely dependent on the application at which the harvester shall be used. It is divided into the following two parts.

2.3.1. The Dielectrics' Effect on the Stored Energy of the Diagonal TENG

The first part is concerned with determining the best combination of the available materials to be used as dielectrics for the diagonal mode attached electrode TENG to achieve the best performance. Table II shows the materials that have been studied with their dielectric constants.

The combinations of studied materials were chosen based upon two criteria; the first is the availability of materials and their cheap and easy fabrication in the solid form. The second is that the materials of each pair are far from each other in the triboelectric series; so that when the system is employed in a real life, a great amount of charges is transferred between them. The Triboelectric series is a list of materials ordered according to their tendency to gain or lose charges [19].

Furthermore, in order not to be limited with the available dielectric materials only with their discrete values of the dielectric constant (ϵ_r), the first part also aims to determine the values of the two dielectric constants that correspond to the system storing the highest amount of energy and thus giving the best performance. The high probability of discovering new materials in the future was a motivation for conducting this study, in which the dielectric constants of the two dielectrics are swept between 1 and 5 and the average stored energy of the configuration from all the angles is calculated to determine the best combination to be used.

Table II. The studied dielectric materials with their constants.

Material	Dielectric constant
PTFE	2
FEP (Fluorinated ethylene propylene)	2.1
Polypropylene	2.2
Polystyrene	2.6
PDMS (Polydimethylsiloxane)	2.75
PMMA (Polymethyl methacrylate)	3
Kapton	3.4
Nylon	4

2.3.2. Diagonal TENG Performance on Unidirectional Charging for a Capacitor

Harvesters converting mechanical energy to other forms can not be used directly because any minor change in the surrounding environment of the harvester leads to the instability of its output. Therefore, they are usually connected to energy storage elements such as capacitors. Accordingly, the second part aims at giving an insight into how capacitors stabilize the output and find the most suitable combination of materials to be used as dielectrics for the diagonal mode TENG that is compatible with the energy storage unit. The developed analytical model of the TENG is used to evaluate its performance when connected to a capacitor as an energy storage unit as shown in Figure 4.

According to Ref. [22], for solving the shown equivalent circuit in case of a capacitive load (C_{load}), the initial conditions of the system are: at $t = 0$, the top dielectric is at $\theta = 0$ position and just starts to move, so charges on TENG electrodes $Q(t = 0) = 0$. Besides, there are no charges on the capacitive load initially $Q_C(t = 0) = 0$. By using Kirchhoff's laws and nodal analysis technique in the circuit, the following equations are reached:

$$V = \frac{-Q}{C_{\text{TENG}}} + V_{\text{OC}} = \frac{Q_C}{C_{\text{Load}}} \tag{35}$$

$$\therefore Q_C = C_{\text{Load}} V \tag{36}$$

$$\because Q_C - Q = Q_C(t = 0) - Q(t = 0) = 0 \tag{37}$$

$$\therefore Q = Q_C = C_{\text{Load}} V \tag{38}$$

By substitution in Eq. (35) at the maximum separation distance at ($\theta = \theta_{\max} = 90$) hence $x \sin(\theta)$ is of maximum value to get the final voltage and charge on the capacitor.

$$\therefore V_{(\theta=\theta_{\max})} = \frac{-C_{\text{Load}} V_{(\theta=\theta_{\max})}}{C_{\text{TENG}}} + V_{\text{OC, max}} \tag{39}$$

$$\therefore V_{(\theta=\theta_{\max})} = \frac{C_{\text{TENG}} V_{\text{OC, max}}}{C_{\text{TENG}} + C_{\text{Load}}} = \frac{Q_{\text{SC, max}}}{C_{\text{TENG}} + C_{\text{Load}}} \tag{40}$$

Therefore, the total energy stored in the capacitor (E_C) can be found as follows:

$$E_C = \frac{1}{2} C_{\text{Load}} [V_{(\theta=\theta_{\max})}]^2 = \frac{C_{\text{Load}} Q_{\text{SC, max}}^2}{2(C_{\text{TENG}} + C_{\text{Load}})^2} \tag{41}$$

With substitution by Eqs. (31), (33):

$$\therefore E_C = \left(C_{\text{Load}} \left[\sigma l x \cos(\theta) + \frac{\sigma l x \sin(\theta)(w - x\cos(\theta))}{(x \sin(\theta) + d_0 + d_{m1} + d_{m2})} - \sigma d_{m1} l + \frac{\sigma d_{m1} l x \cos(\theta)}{(w - x\cos(\theta))} \right]^2 \right) \Bigg/ \left(2 \left[\frac{\varepsilon_0 (w - x\cos(\theta)) l}{(x \sin(\theta) + d_0 + d_{m1} + d_{m2})} + \frac{\varepsilon_0 d_{m1} l}{k_4} + \frac{\varepsilon_0 d_{m1} l}{(k_3 + x\cos(\theta))} + \frac{\varepsilon_0 w l}{k_1} + C_{\text{Load}} \right]^2 \right) \tag{42}$$

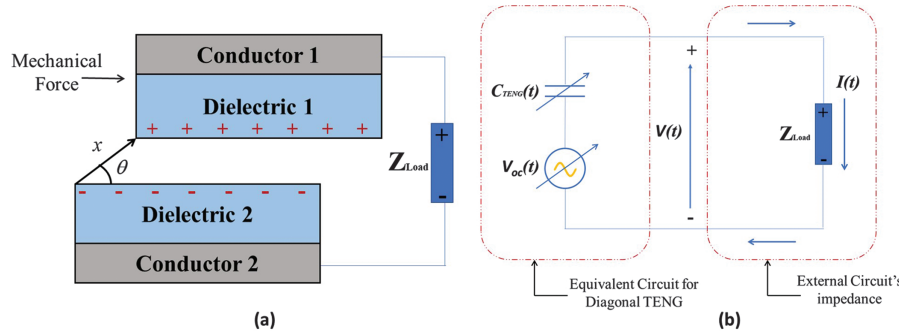

Fig. 4. (a) Diagonal mode attached electrode TENG structure connected to an external load, (b) equivalent circuit model for the whole system.

At the maximum separation distance ($\theta = \theta_{max} = 90°$), the stored energy E_C is reduced to this form:

$$E_C = \left(C_{\text{Load}} \left[\frac{\sigma l x w}{(x + d_0 + d_{m1} + d_{m2})} - \sigma d_{m1} l \right]^2 \right) \Big/ \left(2 \left[\frac{\varepsilon_0 w l}{(x + d_0 + d_{m1} + d_{m2})} + \frac{\varepsilon_0 d_{m1} l}{k_4} + \frac{\varepsilon_0 d_{m1} l}{k_3} + \frac{\varepsilon_0 w l}{k_1} + C_{\text{Load}} \right]^2 \right) \quad (43)$$

Equation (43) is used with the same tribo-pairs of the first part to determine the best combination to be used.

2.4. Verilog-A Model

The $(V - Q - \theta)$ model in (34) along with the relationships in (31, 32) enables TENG modeling by a lumped parameter equivalent circuit model as an ideal arbitrarily time-varying voltage source, $V_{OC}(t)$, serially connected to a capacitor $C(\theta(t))$.[20] Figure 4 illustrates this concept. Regarding the diagonal mode, the upper part, consisting of the upper electrode attached to the upper dielectric, moves in a rotational motion that can be expressed by the equation, $\theta = \omega t$, in which ω is the angular velocity and t is the time. Considering the simple case of a pure resistive network connected to the TENG system via its two electrodes, the $(V - Q - \theta)$ relationship can be expressed as follows:

$$V = R \frac{d}{dt} Q(\theta(t)) = -\frac{1}{C(\theta(t))} \times Q(\theta(t)) + V_{OC}(\theta(t)) \quad (44)$$

Where R is the equivalent resistance as seen at the TENG terminals. The current and voltage waveforms can be obtained at the TENG-load interface by solving $I(t) = d|Q|/dt$ and $V(t) = R(d|Q|/dt)$, respectively. The solution of the integrals in (44) is quite complicated and the particular analytical form of $\theta(t)$ is required. In addition, if more complex loads such as active elements are connected, determining the $(V - Q - \theta)$ relationship requires substituting the previous equation by more complicated ones (e.g., integral or integro-differential equations) whose

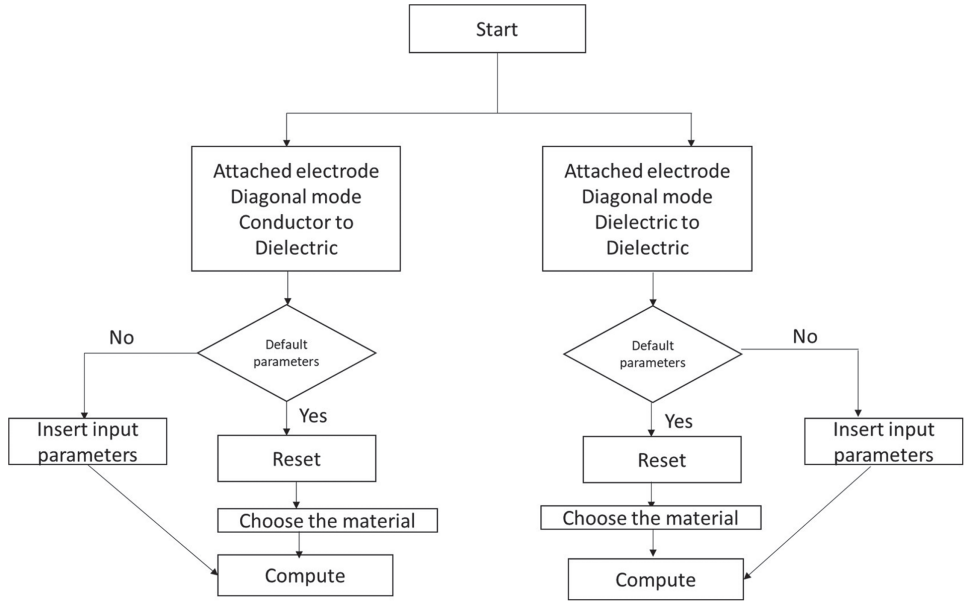

Fig. 5. Flow chart of the CAD tool.

solving analytically is an arduous task and time-consuming if operated by any of the FEM simulation tools. Therefore, a Verilog-A model for the diagonal mode attached electrode TENG is presented as in Ref. [23] to make it easier to incorporate the TENG structure with various complex loads for different applications using different circuit simulation tools (e.g., Cadence Virtuoso). Two cases of pure resistive and pure capacitive loads are incorporated in this work and their results are shown in Figures 10 and 11 respectively.

3. MATLAB CAD TOOL

FEM simulation using COMSOL of the diagonal mode attached electrode TENG is time-consuming especially as the dimensions of the harvester increase. To provide a quicker alternative, a new CAD tool is developed based on the verified full analytical model proposed in this paper (that shows an average error of 5%, 4.3% and 0.88% for the open circuit voltage, short circuit charge and capacitance, respectively). This tool provides a GUI to facilitate the future design of the TENG harvesters for users with less complexity and high speed as compared with COMSOL. It is developed using MATLAB and its operation is shown in the flow chart in Figure 5.

Figure 6 shows a snapshot of the tool operation. Its basic function is to calculate V_{OC}, Q_{SC} and C of a harvester with any set of dimensions and parameters as they are arbitrarily selected by the user. It also offers many additional features such as the reset button that sets the parameters and dimensions to their default values and the plot button that allows for plotting V_{OC}, Q_{SC} or C versus theta to understand the effect of the angle on the harvester's performance. It also generates a set of error messages that makes it easier and more convenient to use the tool correctly such as a range error if the step is inconsistent with the start and end points.

4. RESULTS AND DISCUSSION

4.1. Verification of the Analytical Model

Through scrutinizing the results of the developed analytical model and comparing them with COMSOL results, the analytical model is verified. The FEM results are of an excellent agreement with the analytical model, showing an average error of 5.3%, 4.3% and 0.88% for V_{oc} and Q_{sc} and C respectively due to FEM limitations. The analytical and simulation results, V_{oc}, Q_{sc} and Capacitance are depicted in Figures 7(a)–(c) respectively. Both the open circuit voltage and the short circuit charge exhibit a second order filter response behavior. The results depict a maximum OC voltage of ≈5 V, maximum SC charges of ≈45 pC and a capacitance of value ≈9.2 pF that is almost constant.

4.2. Diagonal TENG Performance Optimization Using Dielectric Materials

Regarding the study of the dielectrics' effect on the performance of diagonal TENG, Table III shows the tribo-pairs used throughout this study with the maximum energy stored in the system of each of them. For the geometry used with the dimensions shown in Table I, the maximum stored energy is at an angle of 80 degrees for all the materials, since the maximum angle is dependent on the geometry only. According to this study, the tribo-pair of Nylon and Kapton combination shows the best performance of the harvester amongst the other pairs used in the literature with a maximum energy of 0.40118 nJ.

For the part concerned with the best combination of ϵ_r to be used even if not corresponding to a known material yet but may be discovered in the future, Figure 8 shows the average energy, according to the developed analytical model, versus the two dielectric constants. Accordingly, the system exhibits a maximum stored energy of 0.3875 nJ at ϵ_{r1} of 5 and ϵ_{r2} of 5. However, this is inconsistent

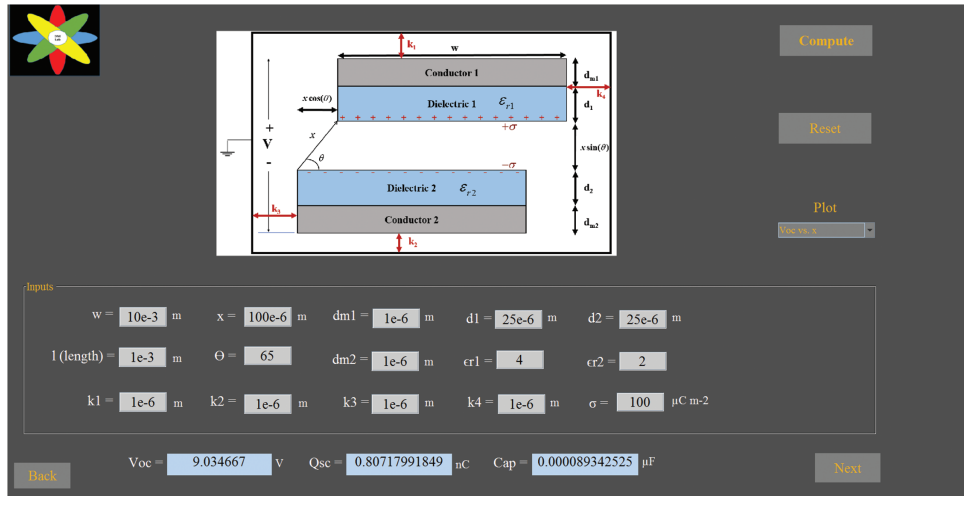

Fig. 6. Setting the parameters and computing the results in the CAD tool.

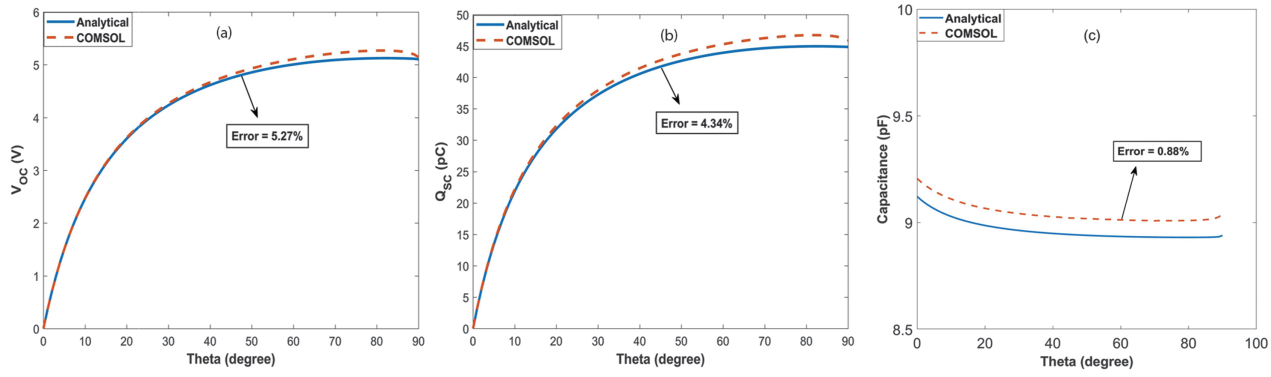

Fig. 7. COMSOL simulation results along with a comparison with analytical model: (a) Open circuit voltage $V_{oc}(\theta)$, (b) short circuit charges $Q_{sc}(\theta)$, (c) total capacitance of the device.

with the triboelectrification phenomenon that requires two different materials to be achieved and thus this combination can not be employed in the harvester. Therefore, the maximum stored energy of the system with two different dielectric constants is shown to be at 0.3866 nJ with the dielectric constants of $\epsilon_{r1} = 5$ and $\epsilon_{r2} = 4.9$.

Regarding the performance of the diagonal mode TENG in charging a capacitor, the output profile of the capacitor stored energy for different dielectric materials with different load capacitances ranging from 1 fF to 1 μF is depicted in Figure 9. The Nylon and Kapton pair gives the best performance compared to the other studied pairs with a maximum stored energy of 97.73 pJ at load capacitance equals to 8.99 pF. The results show that at both high and low load capacitances, the capacitor's stored energy approaches zero. This result is justified as when the load capacitance (C_L) is small, it exhibits very large impedance which is similar to the open circuit case; however, it exhibits limited stored energy (approaches zero) due to the small C_L. On the opposite side, when C_L is large, its impedance will be very small that is equivalent to the short circuit case, but it will also have limited stored energy due to the low voltage applied to it. Furthermore, as depicted in Figure 9, the maximum energy is stored in the capacitor when C_L equals to C_{TENG} which is listed in Table IV for different tribo-pairs and can be easily proved by Eq. (41).

Table III. Maximum energy stored in the system at different tribo-pairs.

Material	Maximum energy (nJ)
Nylon-Kapton	0.40118
Nylon-PMMA	0.39544e
Nylon-PDMS	0.39112e
PMMA-Kapton	0.38611
PMMA-PDMS	0.37656
PMMA-polystyrene	0.37376
Nylon-PTFE	0.37260
PMMA-PTFE	0.35896
Polystyrene-polypropylene	0.35651

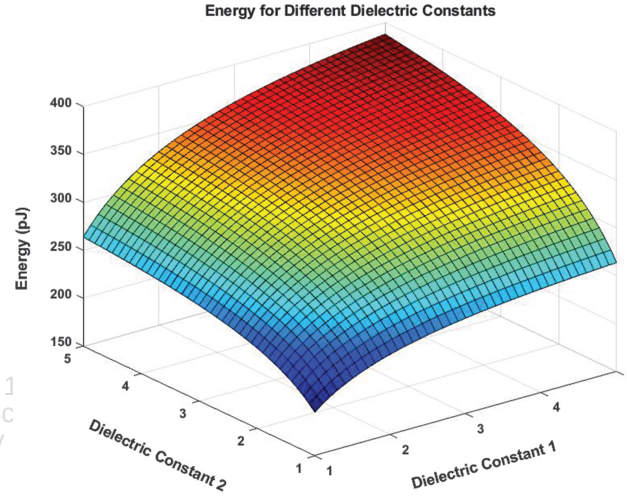

Fig. 8. Stored energy of diagonal TENG versus the two dielectric constants.

4.3. Verilog-A Simulation Results

The accuracy of the developed analytical model was a motivation for constructing a Verilog-A model to investigate the characteristics of the harvester under different loading conditions. Two cases of simple resistive and capacitive loads are investigated in Figures 10 and 11 respectively. The impact of the angle on the I and V is

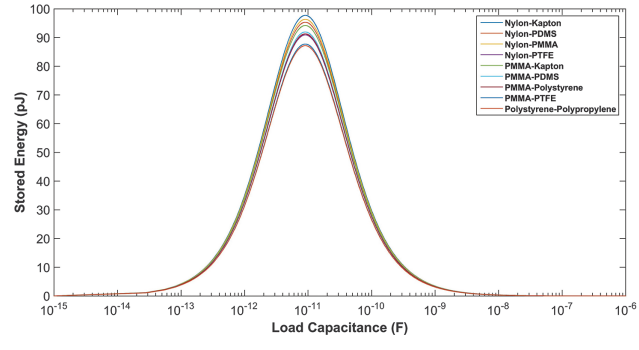

Fig. 9. Profile of the capacitor stored energy for different dielectric materials with different load capacitances.

Table IV. Maximum energy stored on a load capacitor for different tribo-pairs.

Material	Maximum energy (pJ)
Nylon-Kapton	97.7
Nylon-PMMA	96.3
Nylon-PDMS	95.3
PMMA-Kapton	94.2
PMMA-PDMS	91.9
PMMA-polystyrene	91.2
Nylon-PTFE	90.9
PMMA-PTFE	87.7
Polystyrene-polypropylene	87.1

depicted in Figures 10, 11(a) and (b) at different resistance and capacitance values, respectively. The parameters used for conducting the simulations are shown in Table I. Figure 10(a) indicates almost an overdamped second order system response of the voltage against the angle θ for $R = \infty$, which is the case of open circuit voltage. V_{OC} has a peak value equals to ≈5 V at $\theta = 90°$. As the resistance value decreases, the voltage response against θ changes with the voltage peak value receding and reaching zero at $R = 0$, SC condition. On the other hand, the resistor's current shows exactly the opposite response as shown in Figure 10(b). A maximum current of ≈193 pA is observed at at $R = 0$, SC condition, for $\theta = 0$. As the resistance value increase, the output current waveform changes its behavior from an underdamped system into a overdamped system at $R = 100$ GΩ, and eventually reaches 0 at the OC conditions. Figure 10(c) shows the output power in pW swept against resistor values, a peak power of 50 pW is observed at $R \approx 110$ GΩ.

Figure 11(a) indicates an overdamped second order system response similar to Figure 10, however for the capacitance case the behavior is almost the same. The maximum voltage value is found at $\theta \approx 65°$ and $C = 100$ fF, which is the highest impedance since $Z_c = 1/\text{sC}$, to be ≈4.5 V. As for Figure 11(b), a maximum current of ≈194 pA is observed at $C = 1$ μF. As θ goes from 0 up to 90, the current value decreases exponentially and eventually reaches 0. Figure 11(c) shows the stored energy in the capacitor in pJ swept against capacitor value, a peak stored

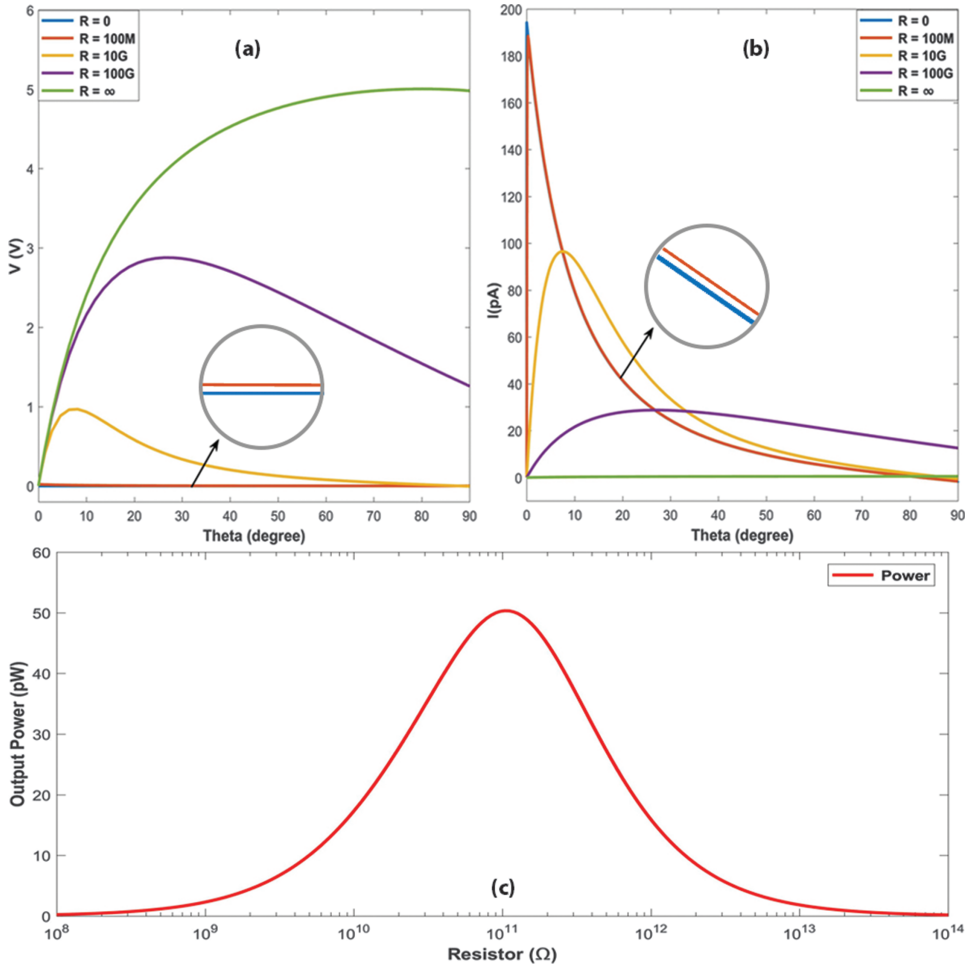

Fig. 10. Verilog-A model of the proposed harvester: (a) $I(\theta)$ versus angle θ at different resistor values. (b) $V(\theta)$ versus angle θ at different resistor values. (c) Average delivered power to the load resistor.

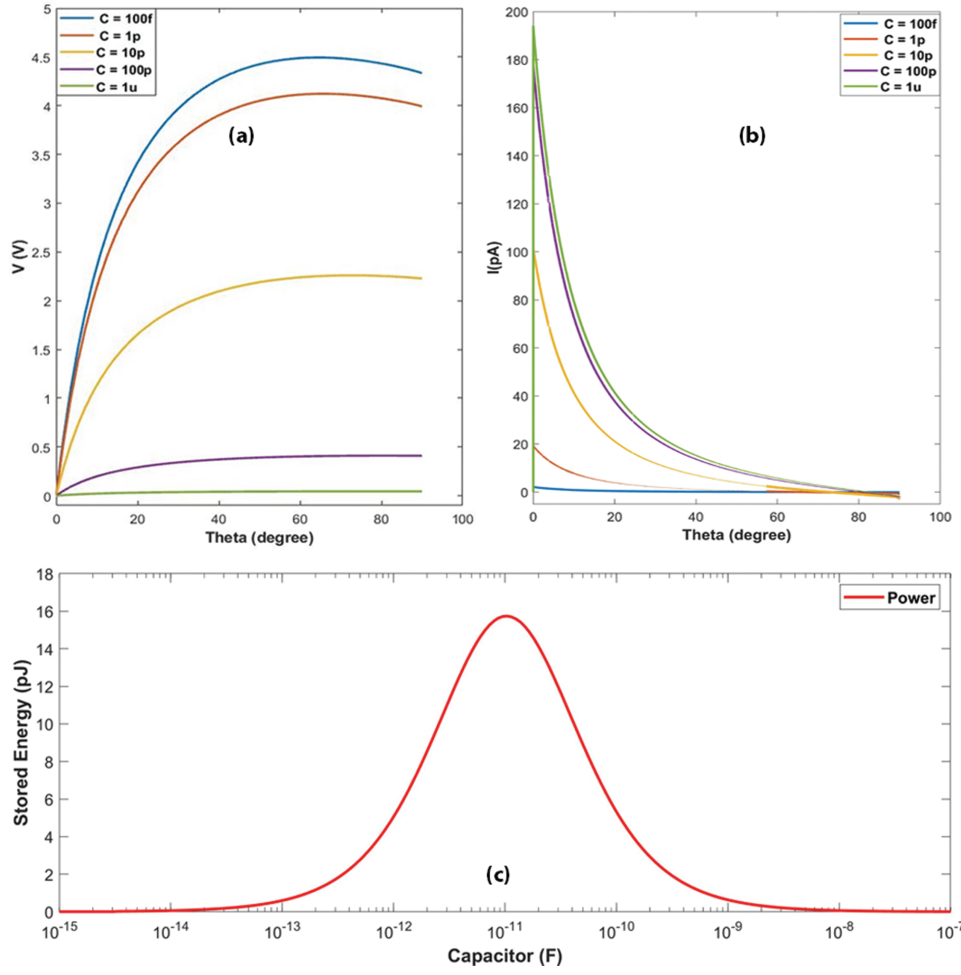

Fig. 11. Verilog-A model of the proposed harvester: (a) $I(\theta)$ versus angle θ at different capacitor values. (b) $V(\theta)$ versus angle θ at different capacitor values. (c) Average delivered power to the load capacitor.

energy of 16 pJ is observed at $C \approx 9$ pF. This actually can be foreseen from Figure 7(c), as the device inherited capacitance ≈9 pF and consequently the matched load must be around the same value according to the maximum power transfer theory. This is also can be proven by (41).

5. CONCLUSION

This paper presents a complete study for the diagonal mode triboelectric nanogenerators based energy harvester. Throughout this study, the first fully analytical model of the diagonal mode of TENG harvester has been thoroughly derived step by step. In addition a COMSOL model has been developed for the harvester. To validate the accuracy of the results obtained from the developed analytical model a comparison has been done with the FEM simulation results. The error between the analytical results and the practical results is less than 6%, which is considered a very promising results compared to contact and sliding mode and other configurations presented in the literature. The results show that the maximum open circuit voltage equals 5 V, and the short circuit charge equals 45 pC. Based on the developed model, a performance optimization study has been performed on the dielectric materials used in the device. The study concluded that, the tribopair of Nylon and Kapton manifests the best performance of the harvester amongst the other pairs used in the literature with a maximum energy of 0.40118 nJ. Based on the derived analytical model, a Verilog-A model has been developed to allow incorporating the device into circuits and assess its performance under different loading conditions. Two cases of simple resistive and capacitive loads are considered in this study. The results show that in case of R_{load} the open circuit voltage, V_{OC}, is equal to 5 V while the short circuit current, I_{SC}, is equal to 193 pA at θ of 0. Also, the peak power is equal to 50 pW for a load resistance of 110 GΩ. As for C_{load}, V_{OC} ≈4.5 V while I_{SC} is equal to 194 pA at theta of 0. Also, the peak power is equal to 50 pW for a load capacitance of 9 pF. Finally, a MATLAB based CAD tool has been developed to allow rapid prototyping and testing of different device parameters on the device performance. A future work to be done is to test the device for more complex loads, derive more

complex circuits and analyze the DC output of the device. This shall help in specifying the best fit application for such device.

Acknowledgment: This work was partially funded by ONE Lab at Zewail City of Science and Technology and at Cairo University, NTRA, ITIDA, ASRT, and NSERC.

References

1. H. Lo and Y. Tai, Parylene-based electret power generators. *Journal of Micromechanics and Microengineering* 18, 104006 **(2008)**.
2. Z. Wang, Triboelectric nanogenerators as new energy technology and self-powered sensors principles, problems and perspectives. *Faraday Discuss.* 176, 447 **(2014)**.
3. S. Roundy, E. S. Leland, J. Baker, E. Carleton, E. Reilly, E. Lai, B. Otis, J. M. Rabaey, P. K. Wright, and V. Sundararajan, Improving power output for vibration-based energy scavengers. *IEEE Pervasive Computing* 4, 28 **(2005)**.
4. A. Khaligh, P. Zeng, and C. Zheng, Kinetic energy harvesting using piezoelectric and electromagnetic technologies state of the art. *IEEE Transactions on Industrial Electronics* 57, 850 **(2010)**.
5. S. Roundy and P. Wright, A piezoelectric vibration based generator for wireless electronics. *Smart Materials and Structures* 13, 1131 **(2004)**.
6. H. Li, C. Tian, and Z. Deng, Energy harvesting from low frequency applications using piezoelectric materials. *Applied Physics Reviews* 1, 041301 **(2014)**.
7. L. Dhakar, Overview of energy harvesting technologies, Triboelectric Devices for Power Generation and Self-Powered Sensing Applications, Springer, Singapore **(2017)**, pp. 9–17.
8. S. M. Niu and Z. L. Wang, Theoretical systems of triboelectric nanogenerators. *Nano Energy* 14, 161192 **(2015)**.
9. S. Boisseau, G. Despesse, T. Ricart, E. Defay, and A. Sylvestre, Cantilever-based electret energy harvesters. *Smart Materials and Structures* 20, 105013 **(2011)**.
10. G. Zhu, C. Pan, W. Guo, C. Y. Chen, Y. Zhou, R. Yu, and Z. L. Wang, Triboelectric-generator driven pulse electrodeposition for micropatterning. *Nano Letters* 12, 4960 **(2012)**.
11. Z. Wang, Triboelectric nanogenerators as new energy technology for self-powered systems and as active mechanical and chemical sensors. *ACS Nano* 7, 9533 **(2013)**.
12. K. Dong, Y.-C. Wang, J. Deng, Y. Dai, S. L. Zhang, H. Zou, B. Gu, B. Sun, and Z. L. Wang, A highly stretchable and washable all-yarn-based self-charging knitting power textile composed of fiber triboelectric nanogenerators and supercapacitors. *ACS Nano* 11, 9490 **(2017)**.
13. G. Zhu, J. Chen, Y. Liu, P. Bai, Y. S. Zhou, Q. Jing, C. Pan, and Z. L. Wang, Linear-grating triboelectric generator based on sliding electrification. *Nano Letters* 13, 2282 **(2013)**.
14. S. Wang, Y. Xie, S. Niu, L. Lin, C. Liu, Y. S. Zhou, and Z. L. Wang, Maximum surface charge density for triboelectric nanogenerators achieved by ionized-air injection: Methodology and theoretical understanding. *Advanced Materials* 26, 6720 **(2014)**.
15. Y. Zi, S. Niu, J. Wang, Z. Wen, W. Tang, and Z. Wang, Standards and figure-of-merits for quantifying the performance of triboelectric nanogenerators. *Nature Communications* 6, Article number: 8376 **(2015)**.
16. G. S. Maximous, A. M. Fatahalla, A. Seleym, T. A. Ashour, and H. Mostafa, A new CAD tool for energy optimization of diagonal motion mode of attached electrode triboelectric nanogenerators, *IEEE International NEW Circuits and Systems Conference (NEWCAS 2018)*, Montreal, Canada **(2018)**.
17. R. AbdEl-Sttar, E. Onsy, G. Maximous, A. Zaky, T. A. Ashour, A. Seleym, and H. Mostafa, Diagonal mode: A new mode for triboelectric nanogenerators energy harvesters, *IEEE International Conference on Next Generation Circuits and Systems (NGCAS 2018)*, Malta **(2018)**, In Press.
18. S. Niu, Y. Liu, S. Wang, L. Lin, Y. S. Zhou, Y. Hu, and Z. L. Wang, Theory of sliding-mode triboelectric nanogenerators. *Advanced Materials* 25, 6184 **(2013)**.
19. Z. L. Wang, L. Lin, J. Chin, S. Niu, and Y. Zi, Triboelectric Nanogenerators, 1st edn., Springer International Publishing AG, Cham, Switzerland **(2016)**, pp. 10–11.
20. A. Zaky, A. Ahmed, P. Ibrahim, B. Mahmoud, and H. Mostafa, In-out cylindrical triboelectric nanogenerators based energy harvester, *61th IEEE International Midwest Symposium on Circuits and Systems (MWSCAS 2018)*, Windsor, ON, Canada **(2018)**.
21. F. S. Bloise, R. M. Ferro, A. B. Rojo, and F. G. Latasa, Static electric field in vacuum, Solved Problems in Electromagnetics, Undergraduate Lecture Notes in Physics, Springer, Berlin, Heidelberg **(2017)**, pp. 71–72.
22. S. Niu, Y. Liu, Y. S. Zhou, S. Wang, L. Lin, and Z. L. Wang, Optimization of triboelectric nanogenerator charging systems for efficient energy harvesting and storage. *IEEE Transactions on Electron Devices* 62, 641 **(2015)**.
23. A. Zaky, M. Shehata, Y. Ismail, and H. Mostafa, Characterization and model validation of triboelectric nanogenerators using Verilog-A, *2017 IEEE 60th International Midwest Symposium on Circuits and Systems (MWSCAS)* **(2017)**.

Endy Onsy

Endy Onsy *studies Nanotechnology Engineering at the University of Science and Technology in Zewail City, 6th of October, Egypt. She is a research intern at Opto-Nano-Electronics Lab (ONE Lab) in Cairo University, currently working on a different TENG type (Single Electrode) with full novel analytical model. Endy has participated, as electrical and control team member, in many robotics and electric competitions such as University Rover Challenge (URC), Minesweepers, and Global Hybrid Electric Challenge (GHEC). Her interests include microelectronics, MEMS, analog and layout design, digital design, embedded systems and robotics.*

Reem Abd El-Sttar

Reem Abd El-Sttar *is currently a student at the university of science and technology of Zewail city in the major of nanotechnology engineering. She also was a STEM school student. She is also an internship student at One lab in Cairo university working on the analytical modeling, optimization and developing verilog-A models of TENGs. She is interested in Analog and digital design, micro/nano fabrication and microelectronics.*

George S. Maximous

George S. Maximous *received his B.S. degree in electrical and communication from the British University in Egypt in 2015. He is a Master student in renewable energy (Triboelectric Nanogenerator) in the British University in Egypt under the supervision of Professor Ashraf Seleym and Professor Hassan Mostafa. His research interests in the energy harvesters including triboelectric nanogenerator, piezoelectric, and solar photovoltaics.*

Ahmed Zaky

Ahmed Zaky *received B.Sc. degree in Nanotechnology and Nanoelectronics (with honors) from the University of Science and Technology at Zewailcity, 6th of October, Egypt, in 2018. He authored 2 papers in international conferences and was a semi-finalist in "MEMS Design Contest" organized by Cadence, X-Fab and Coventor (2017). Currently, he is working as a Research Assistant (RA) at the Center for Nano-electronics and Devices (CND) at the American University in Cairo (AUC), Cairo, Egypt, working on model order reduction and developing algorithms and IPs to EDA software tools for System-on-Chip (SOC) design. His research interests includes EDA algorithms, CAD tools development, IoT hardware security, analog and mixed-signal circuit design, energy harvesting, nano-emerging devices and devices modeling, MEMS, sensing circuits and circuit design with 2D materials.*

Hassan Mostafa

Hassan Mostafa *(S'01-M'11-SM'15) received B.Sc. and M.S. degrees (with honors) in Electronics Engineering from Cairo University, Cairo, Egypt, in 2001 and 2005, respectively, and the Ph.D. degree in Electrical and Computer Engineering in the Department of Electrical and Computer Engineering, University of Waterloo, Waterloo, ON, Canada in 2011. He is currently an Assistant Professor at the Electronics and Communications Department, Cairo University, Cairo, Egypt and also an Adjunct Assistant Professor at the Center for Nano-electronics and Devices (CND) at the American University in Cairo (AUC), Cairo, Egypt. Dr. Mostafa has worked as an NSERC postdoctoral fellow in the Department of Electrical and Computer Engineering, University of Toronto, Toronto, Ontario, Canada. His postdoctoral work includes the design of the next generation FPGA in collaboration with Fujitsu research labs in Japan/USA. He was also working with IMEC, Leuven, Belgium, in 2000. He has authored/coauthored over 130 papers in international journals and conferences and is the author/co-author of 5 published books. Dr. Mostafa is a member of the IEEE Technical Committee of VLSI Systems and Applications (TC-VSA) since 2017. He was the recipient of University of Toronto Research Associate Scholarship in 2012, Natural Sciences and Engineering Research Council of Canada (NSERC) Prestigious Postdoctoral Fellowship in 2011, Waterloo Institute of Nano-technology (WIN) nanofellowship research excellence award in 2010, Ontario Graduate Scholarship (OGS) in 2009, University of Waterloo SandFord Fleming TA Excellence Award in 2008. His research interests include Neuromorphic computing, IoT hardware security, software defined radio, reconfigurable low power systems, analog-to-digital converters (ADCs), low-power circuits, variation-tolerant design, soft error tolerant design, statistical design methodologies, next generation FPGA, spintronics, Memristors, energy harvesting, power management, and optoelectronics.*